IEEE Access
Multidisciplinary | Rapid Review | Open Access Journal

Received June 11, 2019, accepted July 12, 2019, date of publication July 22, 2019, date of current version August 13, 2019.

Digital Object Identifier 10.1109/ACCESS.2019.2930277

Unmanned Aerial Vehicle Impacts on Heat-Strengthened Glass

SANG EON LEE, JAE-WOOK JUNG, YOUNGJUN CHOI, YOON-JIN YOON, (Member, IEEE), AND JUNG-WUK HONG

Department of Civil and Environmental Engineering, Korea Advanced Institute of Science and Technology, Daejeon 34141, South Korea

Corresponding author: Jung-Wuk Hong (j.hong@kaist.ac.kr; jwhong@alum.mit.edu)

This work was supported in part by the Ministry of Land, Infrastructure, and Transport of Korean Government under Grant 18USTR-B127901-02, and in part by the National Research Foundation of Korea (NRF) through the Korea Government (MSIT) under Grant 2018R1A2A1A05019453.

ABSTRACT Increasing demand for small unmanned aerial vehicles (UAVs) in the logistics and rescue fields, which are closely related to urban environments, has been accompanied by an increase in impact risk to people and property. However, safety regulations for small UAVs in urban areas have not yet been well established, and there are very few studies investigating the collisions between UAVs and building structures that could occur in an urban area. In this study, experimental and numerical investigations are conducted to evaluate the damage resulting from a UAV collision with heat-strengthened glass, a widely used building exterior cladding. Commercially available UAVs were impacted into a series of glass panels at various speeds and angles. The collision processes were recorded with a high-speed camera, and the impact forces of the UAVs were measured using dynamic force sensors. A numerical model of the UAV was then developed to simulate the impacts using the finite element method and verified by comparison with the experimental results. The collision tests performed in this study are expected to provide primary data for establishing UAV safety regulations, and the verified numerical model can be applied to evaluate various collision scenarios for the different UAVs.

INDEX TERMS Unmanned aerial vehicles, finite element methods, risk analysis, force measurement.

I. INTRODUCTION

The use of small unmanned aerial vehicles (UAVs) has proliferated in populated areas in recent years. However, this emerging industry has faced significant challenges in establishing regulations and standards to ensure the safety of UAV operation [1]. Such challenges have led aviation safety regulators to undertake and promulgate a comprehensive risk assessment [2], [3]. A priority task of this risk assessment is to recognize what risk factors exist and how to classify them. Two primary hazards have thus far been identified:

1) Collision between a UAV and another aircraft.
2) Controlled or uncontrolled impact of a UAV with people or structures on the terrain [4], [5].

Some research on the former hazard has been reported. Song and Schroeder investigated a method for quantifying risk using a computational method to evaluate UAV ingestion into a high-bypass commercial jet engine [6], [7]. Additionally, the European Aviation Safety Agency (EASA) and Civil Aviation Administration of China (CAAC) have conducted collision tests to estimate the damage to cockpit windshields by UAV strikes [8], [9]. Recently, more studies have concentrated on the latter hazard as the use of small UAVs has significantly increased in urban areas. Many emerging UAV applications such as logistics and surveillance require safe operation of small UAVs in densely populated cities [10]. Accordingly, UAV collision avoidance algorithms have been intensively studied. There are various collision avoidance systems for UAVs in accordance with the installed sensor types and selected avoidance algorithms [11]. However, numerous defects including signal loss, insufficient battery capacity, and unskilled operation still remain. Besides, in urban areas, small UAVs are also particularly vulnerable to wind gusts around high-rise buildings [12]. A variety of sensors and high-performance components are required to inhibit all the risks associated with extensive UAV usage, but such a complete collision avoidance system raises costs and difficulty in implementation. Even with such collision avoidance systems, both people and property can be exposed to potential UAV crashes or falls.

The associate editor coordinating the review of this manuscript and approving it for publication was Zhenbao Liu.

To approach this problem proactively, researchers have estimated the extant risks of UAV operation. Dalamagkidis *et al*. computed the probabilities of fatalities and the fatality rates with respect to UAV ground impact using a risk-based assessment [13], [14]. La cour *et al*. asserted that a UAV mass greater than 250 g would be lethal to a human being [15]. They also proposed a preliminary methodology capable of calculating an optimized flight path and altitude for a specific UAV to minimize the probability of fatalities [16]. Geofencing, based on a topological method, has been another approach to reduce the risks due to UAV operations in densely built-up areas. Many countries stringently regulate the minimum distance UAVs must maintain from people and human-made structures, ranging from 30 m to 150 m. However, it is predicted that these conservative restrictions may restrain the airspace available to UAVs, potentially causing aerial traffic congestion in the future. To accommodate the potential for increasing UAV numbers, a more practical and rational geofence is necessary to ensure usable or operable flight [17]. Although researchers have endeavored to mitigate the potential risk due to the operation of small UAVs in theory, a certain degree of predictable risk is unavoidable [18]. In essence, the problem is that commercially available UAVs currently do not have sufficient control autonomy to operate without some degree human supervision [19].

Realizing the limits and high uncertainty of theoretical studies, researchers have garnered extensive data that accurately define the potential UAV damage to people and property through experiments [20]. There are two notable studies that have measured the impact energies and fatalities due to collisions between small UAVs and people. Koh *et al*. suggested that weight thresholds be limited to within a range harmless to people, determined by falling impact tests from various heights onto a human dummy [21]. Campolettano *et al*. performed falling impact tests as well as airborne flight tests. In the airborne flight tests, the effectiveness of the tests was limited by extensive energy dissipation during impact on account of the geometric features of the human dummy used, leading to a non-centric effect [22].

Few studies focusing on UAV damage to structures have been reported. When operating small UAVs in urban areas, one of the most significant hazards is a collision with a building. Laminated glass or monolith glass cladding is a nearly ubiquitous material on the exterior of buildings in South Korea, and it is more vulnerable to airborne flight impact than other structural materials. Laminated glass is typically made up of two or more layers of glass panels sandwiching one or more multiple layers of polymer sheeting. Several types of glass including float glass, heat-strengthened glass, and tempered glass are used as the glass layers depending on their application [23]. If a UAV were to penetrate a glass window, it would pose a severe threat to the people inside the building. Despite the recognition of such a lethal risk, there have been few studies on the impact risk assessment of UAVs against glass. Both ASTM [24] and US DoD UFC [25] standards indicate that such laminated glass windows are nominally 6.75 mm thick with two 3 mm thick glass panels bonded with a 0.75 mm thick polyvinyl butyral (PVB) interlayer. Accordingly, in this study, the effects of a UAV impact on heat-strengthened glass panels of different thicknesses (3 mm, 5 mm, and 8 mm) were evaluated. Heat-strengthened glass panels were used instead of laminated glass because the interaction between the glass and the interlayer in laminated glass could result in a lower transfer of energy from the UAV impact to the force sensors. In the experiments conducted in this study, the applied forces on and failure shapes of the glass panels were obtained using dynamic force sensors that measured the time-dependent force at the corners of a rectangular glass target and a high-speed camera that recorded the collision responses at a speed of 6,900 frames per second (fps), respectively. The fracturing or non-fracturing of the glass was also observed under various impact conditions by changing the impact velocities and angles of human-operated UAVs. Using the results of these tests, we then propose a probability of failure function by modifying the blunt criterion (BC) and apply it using a finite element analysis that is demonstrated to be in good agreement with the experimental results. This verified numerical model will be useful for estimating the risk of fatality or damage due to structure impact by many different types of UAVs.

II. THEORETICAL BACKGROUND

A. INJURY CRITERIA

There are various criteria for predicting the damage not only to UAVs but also due to collisions between moving objects with mass and velocity. A moving object has both momentum and kinetic energy, and thus generates an impact force during a collision. In this section, the injury criterion used to estimate the damage to the target is probabilistically established based on the physical parameters of the UAV and target.

1) ABBREVIATED INJURY SCALE (AIS)

The abbreviated injury scale (AIS) is a widely-used injury criteria that classifies the probability of a person being killed in a traffic accident. It was the first anatomical scoring system proposed in the 1970s when the trauma system was initially established in the United States. The AIS was created in 1971 to define the types and severity of car traffic accidents, and the current AIS code has been refined through five revisions. The AIS code describes damage and degree of severity on a scale from 1 to 6, where AIS 1 indicates minor injuries, AIS 5 indicates the most critical injuries, and AIS 6 indicates injuries considered impossible to survive. Many studies have been conducted to convert physical quantities such as kinetic energy, momentum, or impact force into the AIS scale [21]. In this paper, the potential risk of UAV collision can also be presented based on the AIS scale by indirectly calculating it by use of the kinetic energy and impact force, even though the AIS is typically only calculated for impacts with human subjects.

2) BLUNT CRITERION

The blunt criterion (BC) is a factor that predicts the probability of fracture considering the characteristics of the projectile and target based on the kinetic energy. However, it is difficult to accurately estimate damage using only kinetic energy. When a projectile collides with an object, the resulting damage depends on its size, shape, and impact position. Therefore, the criterion is written as follows:

$$\mathrm{BC} = \ln\left(\frac{MV^2}{2W^{1/3}TD}\right), \tag{1}$$

where M is the mass of the projectile (in kg), V is the velocity of the projectile (in m/s), D is the diameter of the projectile (in cm), W is the mass of the impacted body (in kg), and T is the thickness of the body wall (in cm).

The correlation between the BC predictor and fracture could potentially be estimated using logistic regression [26]. In this study, the BC is utilized to predict the destruction of glass panels due to UAV collisions. Because the BC is calculated considering the diameter of the projectile, we can modify the BC for the UAV collisions by accommodating the kinetic energy of the UAV and size of the target structure as follows:

$$\mathrm{BC}_{\mathrm{UAV}} = \ln\left(\frac{mv^2}{2bht}\right), \tag{2}$$

where m is the mass of the UAV (in kg), v is the velocity of the UAV (in m/s), b and h are the width and height of glass panel target (in m), respectively, and t is the thickness of the glass panel (in mm).

B. AIRCRAFT IMPACT SIMULATION

1) RIERA METHOD

Aircraft collision experiments are difficult to perform directly due to their extremely high cost. Therefore, aircraft collision tests are typically focused on specific components such as the engines or fuel tanks. The responses to collision are then predicted based on numerical analyses. Riera proposed a method for estimating the force due to an aircraft strike using the law of momentum conservation [27] as follows:

$$P(t) = P_b(x(t)) + \mu(x)v^2(t), \tag{3}$$

where $x(t)$ is the collision length of the aircraft, $\mathrm{P}_b(x)$ is the static load of the airframe (excluding the engine) axially located at a position x, $\mu(x)$ is the mass per unit length at position x, $v(t)$ represents the speed of the aircraft, and $P(t)$ is the reaction force between the collapsing aircraft and a rigid surface. The load functions proposed by Riera include several assumptions, including that the target surface is rigid, the longitudinal direction of the aircraft is perpendicular to the target surface, and the aircraft material exhibits perfectly plastic behavior. Sugano *et al.* improved this load function by applying a strength reduction factor α to Riera's equation with a suggested value of 0.9 [28] as follows:

$$P(t) = P_b(x(t)) + \alpha\mu(x)v^2(t) \tag{4}$$

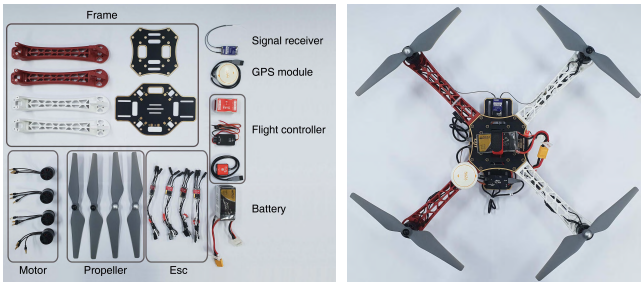

(a) (b)

FIGURE 1. (a) Components and (b) assembly of the DJI-F450 UAV.

The modified Riera method has the advantage of estimating the impact force of the aircraft using the initial velocity, stiffness, and mass distribution of the aircraft, but it is difficult to apply this method to the prediction of UAV impact force because the UAV does not perpendicularly collide with the face of the structure.

2) UAV-TARGET INTERACTION ANALYSIS

The Riera method indirectly calculates the impact force through its assumptions, while it is able to directly calculate the impact force of an aircraft using a finite element method (FEM) analysis. In structural engineering, an FEM analysis solves a mathematical model by iterative numerical approximation using defined material properties and boundary conditions [29]. In order to verify a developed numerical analysis, the analysis results must be compared with those of an experiment or different analytical solution. Such a numerical model is useful for obtaining the results of many different collision scenarios under various parameters without incurring additional cost. Additionally, it is difficult to conduct collision tests with an exact UAV collision velocity and angle, while such variables are easily controlled in a numerical simulation.

III. EXPERIMENTAL SETUP AND RESULTS

A. EXPERIMENTAL SETUP

The multi-purpose, widely used DJI-F450 UAV model was selected as the impact source in this study. This DJI UAV weighs 903 g with a wheelbase length of 450 mm and four propellers. Fig. 1 shows the components of the DJI-F450, including the arm frames, rotors, propellers, signal receiver, GPS module, flight controller, and battery. The UAV was configured using the F450 kit including DJI 2312E rotors with a velocity constant of 960 kV, E 430 lite electronic speed controllers (ESC), and the DJI 9450 self-tightening propellers. The DJI Naza-M Lite flight control system, which includes a 3-axis gyroscope, 3-axis accelerometer, and barometer in its main controller, was used as the UAV flight controller and provided three control modes: attitude, GPS, and manual. In attitude mode, the flight controller automatically maintains the altitude of the aircraft, GPS mode maintains both the altitude and position, and manual mode provides automatic

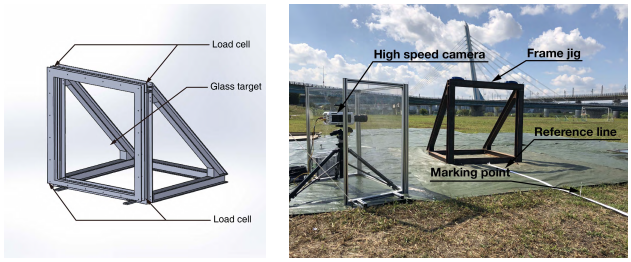

FIGURE 2. (a) Three-dimensional configuration of the target jig and (b) field installation of the target jig and high-speed camera.

calibration but allows flight without any restrictions. Considering the need for an accurate collision at the center of target, attitude mode flight was selected for use in this study.

The Naza-M Lite flight controller has a maximum tilt angle of 35° in attitude mode for stable flight, and the maximum speed during the experiment was about 18 m/s. A Futaba 18SZ transmitter and a TAROT 8-channel Futaba S-FHSS compatible receiver were used for communication and control. A Tattu 4-cell Lithium polymer battery, 14.8 V with a capacity of 1550 mAh, was mounted in consideration of the requirements of the flight controller, rotor, and ESC. A relatively light and small capacity battery was used because the experiments did not require a long flight time.

The jig structure used to hold the collision target, shown in Fig. 2, consisted of two steel frames designed to mount the heat-strengthened glass panel and a support structure comprised of H-beams to hold the steel frames. The glass target was 1240 mm × 1240 mm and the various thicknesses of the target glass were accommodated using various bolt lengths. The support structure was made of nine SS400 steel H-beams with a nominal size of 100 mm × 100 mm and assembled by bolting. Fig. 2a shows the three-dimensional geometry of the jig structure designed by the commercial modeling program SolidWorks. The steel frames sandwiching the glass were installed in front of the support structure. A total of four force sensors were then installed between the back of the steel frame and the support structure. Linear guides were placed at the bottom of the rectangular frames to induce sliding, minimizing the kinetic energy loss due to the frictional force during impact.

Using a high-speed camera (Phantom V611), the interaction between the glass and UAV was recorded at a speed of 6,900 fps from the diagonal, as shown in Fig. 2b. Another digital camera was located to the side of the target to measure the impact velocity and angle at 240 fps during the collision. A total of six poles, placed on a reference line at 1 m intervals for 5 m ahead of the target, were used to obtain the velocity. The impact velocity was determined by observing the travel distance of the UAV relative to the poles in each frame captured by the camera. The reference line was installed on the right side in advance of the target structure to help direct the UAV to collide at the center of the target.

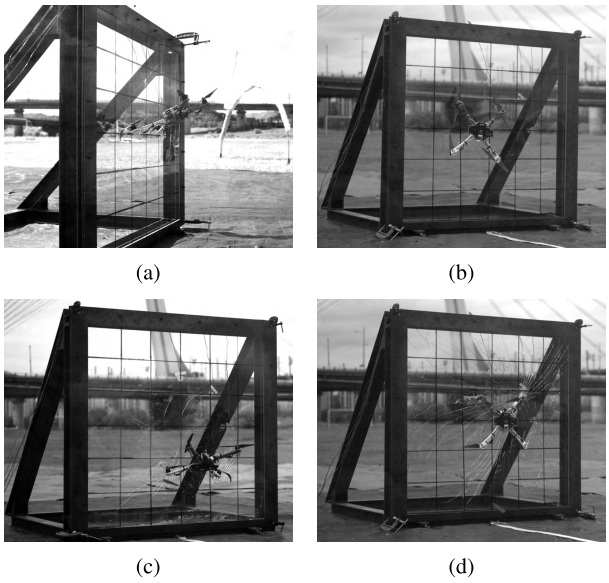

FIGURE 3. Images captured by the high-speed camera before and after the UAV collision with the glass panel: (a) Tilting UAV immediately before front rotor collision; (b) unbroken target panel after front and rear rotor collisions at low UAV velocity; (c) fracture due to front rotor collision, which was frequently observed for thin panels; and (d) fracture due to rear rotor collision, which was frequently observed for thick panels.

The impact loads were measured by force sensors. Four PCB 208C05 dynamic force sensors made by PCB Piezotronics with a compressive force capacity of 22.24 kN were placed at the corners of the target to measure the dynamic load during impact. When the force sensors were compressed, an electrostatic charge proportional to the external force was generated, and output as a voltage signal. This signal was then transmitted to a dynamic data logger at a sampling rate of 5 kHz. The data measured by the four force sensors were integrated to calculate the total impact force due to the UAV collision.

In order to protect the high-speed camera and the dynamic data logger from the fragments of glasses, shockproof and transparent walls made of polycarbonate material were installed.

B. EXPERIMENTAL RESULTS

The experimental results are comprised of an analysis of the glass fracture shape due to UAV collision, the development of a failure probability function, and an impact force analysis. First, Fig. 3 shows images from the high-speed camera, which was able to obtain one image every 144 μs, just before and after the UAV collision with the glass target.

Fig. 3a was taken before the collision from the side of the target structure, in which it can be seen that the UAV collided with the glass panel at an angle, and the front two rotors touched the surface of the glass simultaneously. No destruction of the glass due to the rotation of the propellers was observed in these experiments. While sharp propellers can damage soft tissues such as skin, propellers of small UAVs rarely cause direct damage to structure exteriors such as

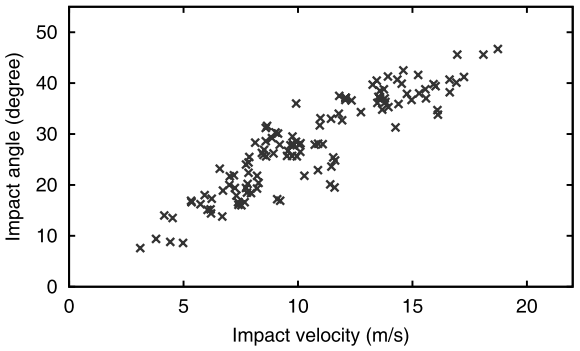

FIGURE 4. Correlation between tilting angle and velocity of UAV just before the collision to the target.

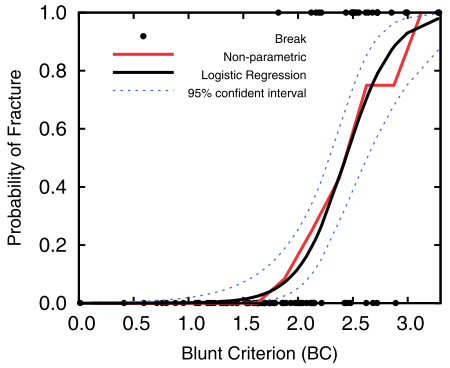

FIGURE 5. Risk function for the prediction of fracture based on the blunt criterion.

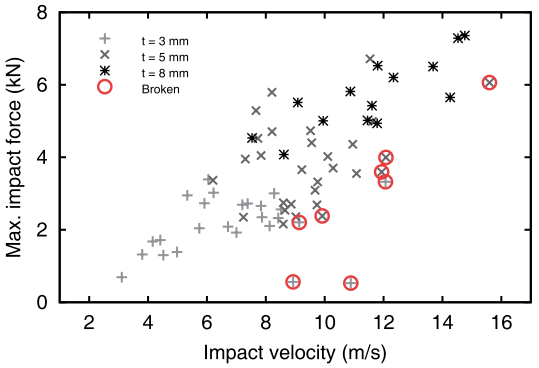

FIGURE 6. Relationship between maximum impact force and impact velocity in UAV impact tests. The red circles represent the cases in which the target glass was broken.

glass or concrete. Instead, it has been observed that the front propellers behave like a bumper during impact with a hard surface, breaking or bending between the relatively stiff rotor and the impacted structure. Fig. 3b shows the moment of rear rotor collision after the UAV had rotated forward due to the front rotor collision. For experiments with sufficiently thick glass and low impact velocity, neither the front or rear rotor collisions resulted in glass panel fracture.

Fig. 3c shows the failure of a thinner glass panel due to front rotor collision. In this case, the people inside the building would be exposed to risk not only due to collision impact causing unstable flight and malfunctions of the UAV, but also due to the fragments of glass caused by the impact. Fig. 3d indicates that glass panel damage occurred as a result of the rear rotor collision after the flipping motion of the UAV when the front rotor collision did not break the glass. The failure of the glass due to rear rotor collision was observed when the UAVs impacted the glass at high speed. The velocity and tilting angle of the UAV were found to have a linear proportional correlation, shown in Fig. 4. As the tilting angle increased, the impact force of the rear rotor was larger than that of the front rotor on account of the substantial angular momentum generated by the flipping motion. Therefore, in the case of thicker glass panels, failures were mainly observed due to the rear collision shown in Fig. 3d because thicker glass requires a higher kinetic energy to break.

The fracture probability of the glass panel was predicted based on the modified blunt criteria in Eq. (2). Due to the inherent characteristics of heat-strengthened glass, the strength of each glass panel was not consistent. The characteristics of the glass also depends on the temperature, humidity, and variation in the collision position during each impact. Therefore, a statistical approach to capturing the fracture probability was required. In Fig. 5, the black dots at the top and bottom of the horizontal axes represent the results of 98 collision tests. For each collision, the BC was calculated using Eq. (2) and the probability of fracture was set to 1 if the glass panel was broken and 0 if it was not. A logistic regression was then performed using non-commercial statistical computing software R with the results shown in Fig. 5 for a 95% confidence interval. The probability function of fracture was calculated by:

$$P = \frac{1}{1 + e^{-q(\mathrm{BC})}} \tag{5}$$

where P is the probability of fracture and $q(\mathrm{BC}) = -4.5854 \times \mathrm{BC} + 11.1656$. The non-parametric model in Fig. 5 was generated using the certainty method model proposed by Mertz [30]. The significance level of the logistic regression was set to $p < 0.05$, and the p-value of the model was $3.37e^{-06}$, which indicates that the model was statistically significant. From the probability of fracture function, a risk of failure of 50% was calculated when BC = 2.435.

Fig. 6 shows the maximum measured impact forces with respect to the velocities of the UAVs. In the initial stage of the experiment, 33 tests were performed without force sensors to determine the critical velocity at which the destruction of the glass targets began to occur. These data were only used to estimate the failure probability function of the glass targets. Then, 65 experiments were performed with the force sensors installed to measure the impact load, and the results of these tests are plotted in Fig. 6, in which the red circles represent the occurrence of a fracture. Note that the measured maximum forces at fracture were smaller than the forces in other tests, indicating that nontrivial portions of the kinetic energies of the UAVs were transferred to the fracture energies and kinetic energies of the fragments.

The AIS criteria are used to classify human injury level when a moving object directly impacts a human body. Although this study is focused on UAV collisions with the exterior glass of a structure, it can be indirectly estimated the particular AIS level corresponding to its measured impact force and kinetic energy of the UAV, providing an additional quantification of the severity of impact. The maximum speed of the DJI F450 UAV in this experiment was 18 m/s as shown in Fig. 4. Sturdivan *et al.* suggested an energy threshold of 49.5 J for AIS 3 and 99 J for AIS 4 [26]. These energy values are equivalent to UAV velocity thresholds of 10.5 m/s for AIS 3 and 14.8 m/s for AIS 4. Thus, the 903 g UAV can be indirectly predicted to pose a risk level between AIS 3 and AIS 4 in terms of its initial kinetic energy. For an AIS skull fracture test, the force thresholds were 5.5 kN for AIS 3, and 11 kN for AIS 4 [31]. In this research, the maximum impact force was 7.8 kN as shown in Fig. 6, which is classified as AIS 3. The force and energy thresholds of the AIS criteria suggested in past research have been defined through skull fracture tests, and so it is difficult to directly apply the AIS criteria to the experiment results performed with impacts to a glass structure. However, as for the results of these experiments, it is expected that the impact of the 903 g UAV could represent an AIS 3-4 hazard.

For tests conducted using 3 mm thick panels at velocities from 3 to 6 m/s, the velocity and maximum force were proportional. In these tests, the maximum load was observed at the moment of front rotor collision from images captured by the high-speed camera. For tests conducted using 8 mm thick panels and velocities greater than 12 m/s, the maximum load was measured at the moment of rear rotor collision using images from the high-speed camera. For tests conducted on 3, 5, and 8 mm thick panels at velocities between 6 m/s and 12 m/s, the maximum impact force was observed to be evenly dispersed by repeated collisions. In this velocity region, all collisions were conducted twice.

Fig. 7 illustrates the time-dependent force exerted on the force sensors when the UAV collided with the 8 mm thick panel at a velocity of 13.7 m/s. The time t_1 represents the moment at which the front propellers reached the glass panel, t_2 represent the time at which the front rotors collided with the panel, and t_3 represents the time at which the rear rotors collided with the panel. Vibration of the panel was observed due to the rotation of the propellers, and the load was observed to increase immediately after each collision. Although the maximum force was observed during the rear rotor collision, the impact force due to the front rotor collision was also considerably large. For velocities between 6 m/s and 12 m/s in Fig. 6, the maximum force can be observed to be widely distributed due to the nature of the impacts depending on the UAV velocity and angle. Therefore, a numerical approach is required to determine the effects of these variables in detail. In this study, only the cases in which the velocity and impact angle exhibited a linear correlation, as determined from Fig. 4, were numerically investigated. In practice, as UAVs may confront unexpected climatic conditions such as wind gusts and turbulence during the flight, it is difficult to assure that UAVs always cruise in the linear correlation of the impact velocity and angle. Since such unexpected conditions are difficult to implement in experiments, numerical modeling is essential to complement this limit. Consequently, we verified the numerical model by comparing the results of the experiments with those of the numerical simulation in Section IV.

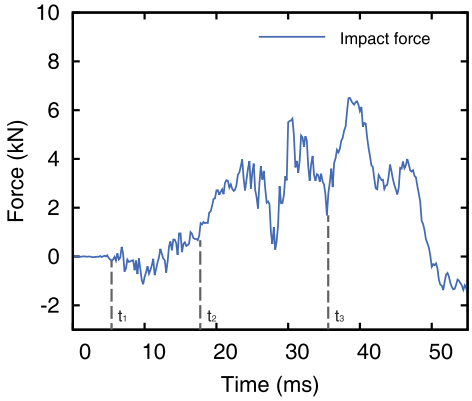

FIGURE 7. Impact force-time history of force sensor data (t = 8 mm and v = 13.7 m/s).

IV. NUMERICAL ANALYSIS

The important variables determining the characteristics of the UAV crash scenario are the type and weight of the UAV, the impact velocity, the impact angle, and the nature of the impact target. Evaluating the relative influences of all these variables simultaneously using field tests is a demanding task. The numerical approach applied in this study has the advantage of addressing such field test limitations and is capable of estimating risk under a wide variety of crash scenarios. In this study, the UAV impacts were evaluated using FEM analyses and verified by comparison with the experimental results. The numerical models were developed based on the DJI-F450 UAV model and the target glass used in the experiments. The nonlinear finite element analysis platform LS-DYNA [32], which has a large library of material models and element formulations, was employed to perform the UAV impact analyses.

A. NUMERICAL MODEL

1) UAV AND TARGET MODEL

The 3D geometry of the DJI-F450 UAV established in SolidWorks was converted into a finite element mesh for the numerical analysis using LS-DYNA and is shown in Fig. 8. The main components of the UAV that affect the collision response are the frame arm, main body, battery, and rotors. Ineffective components such as the ESC, signal receivers, GPS module, flight controller, and wires were omitted for modeling convenience, and the total weight of the omitted parts was added to the weight of the battery. The entire UAV model was discretized by 150,000 hexahedral elements of about 2 mm, except the propellers, which consisted

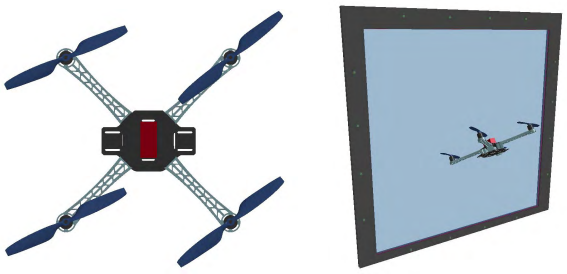

(a) (b)

FIGURE 8. (a) Three-dimensional configuration of the UAV and (b) UAV impact with simulated target frame.

of 10,000 tetrahedral elements of 3 to 4 mm. The material properties of the UAV components are summarized in Table 1. The mechanical behavior of each material was described using the plastic kinematic material model, which employs a bi-linear elasto-plastic constitutive relationship. Components of the UAV were constructed as separate parts and assembled in the model by applying the tie function at their contact surfaces.

The numerical models of the jig and target consisted of a glass panel, a pair of steel frames, and bolts for mounting the frames to the glass panel. The glass panel was located between the two steel frames and fixed by bolts using the contact function so that these elements behaved identically. The different thicknesses of glass (3 mm, 5 mm, and 8 mm) and the steel plates used in the experiment were modeled using hexahedral elements. For the boundary conditions, all degrees of freedom of the four nodes at the location of the force sensors were restricted, and the time histories of the impact forces were extracted from these nodes during the analysis.

At the beginning of the collision response, the front propellers collided with the target glass and warped. After the front rotors crashed into the glass, the UAV rotated forward and the rear rotors collided with the glass. Thus, the front propellers were destroyed at the beginning of the collision and lost their momentum. However, the rear propellers preserved their momentum until they collided with the glass. Accordingly, during the collision, the rear parts of the UAV further accelerated and collided with the glass at a significantly higher velocity than the initial impact velocity. In order to take this into consideration, an additional acceleration was applied to the rear rotors.

Glass strength depends on the presence of micro-flaws on the glass surface induced by the manufacturing process and weathering during the service life of the glass [33]. Thus, the glass strength varies and is generally assumed to follow a Weibull distribution. Theoretically, the strength of glass is between 15 GPa and 21 GPa [34], but is often less than 100 MPa in reality. To address this discrepancy, Zhang *et al.* conducted a parametric study with respect to several different glass strengths (60 MPa, 90 MPa, and 120 MPa) [23]. Since the strength of glass is hardly known, we assumed it to be 80 MPa; the maximum failure strength commercially available [35]. The elastic modulus of the glass used in the field test was calculated from the density and wave velocity, which were measured from a 7.7-mm thick laminated glass plate sample. The wave velocity was calculated by measuring the time delay of the wave passing through this glass plate, as shown in Fig. 9.

B. NUMERICAL RESULTS

Using the detailed FEM model of the UAV and target, two representative collision cases were selected and their time histories of impact forces were analyzed for comparison with the experimental results to verify the accuracy of the numerical model. The FEM-modeled UAV impact force was evaluated for thick glass panels in which no fracture occurred, and for thin glass panels that were destroyed in the experiments. The sensors used to measure the dynamic force during the collision are shown in Fig. 10a. Due to the bending of the target during the collision, shown in Fig. 11, the impact force was not accurately applied solely in the axial direction of the force sensor; a normal force and tangential force were also simultaneously applied, as illustrated in Fig. 10b.

1) UAV IMPACT SIMULATION WITH THICKER GLASS PANEL

To verify the numerical UAV model, the experimentally measured time history of impact force was compared with the numerical results. In this case, the numerical analysis was performed for an impact velocity of 13.7 m/s, an impact angle of 36.6°, and an 8 mm thick glass target.

The impact forces were extracted from the nodes at the four corners of the target model where the force sensors were located. The normal force, shown in Fig. 12a, exhibits a slightly negative value immediately after the collision and a total of four peak values as the respective pairs of front and rear rotors collide with the target. The peak values can be distinguished separately because the front and rear rotors did not collide simultaneously in either the experiment or the simulation. The tangential force, shown in Fig. 12b, gradually increases until 30 ms after the collision, then decreases thereafter. It is posited that the tangential force increases with

TABLE 1. Material properties of DJI F450.

	Frame Arm (PA66-GF)	Frame Board (PCB)	Propeller (DJI-Blades)	Battery (Li-Po)	Rotor (Copper)
Density (kg/m^3)	1370	2700	1520	3406	3450
Young's Modulus (GPa)	10	68.9	1.7	0.5	117
Poisson's ratio	0.35	0.33	0.35	0.30	0.34
Yield Strength (MPa)	190	276	39	30	70

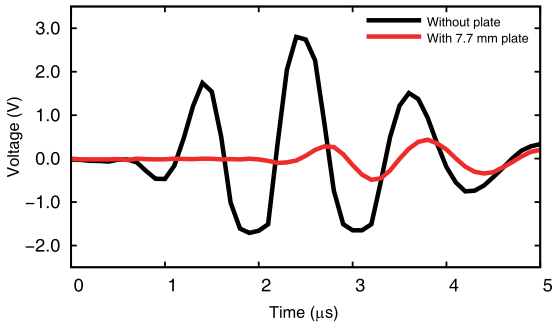

FIGURE 9. Time delay of the wave passing through the glass plate sample.

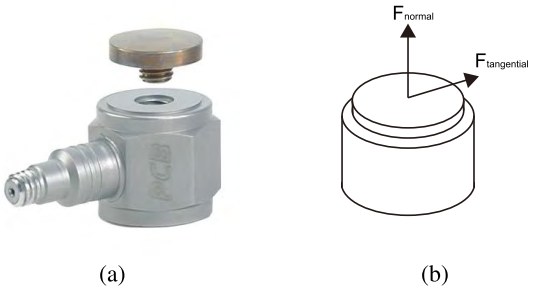

FIGURE 10. (a) Dynamic force sensor (PCB 208C05, PCB Piezotronics Inc., USA) and (b) schematic of the tangential and normal force on the force sensor.

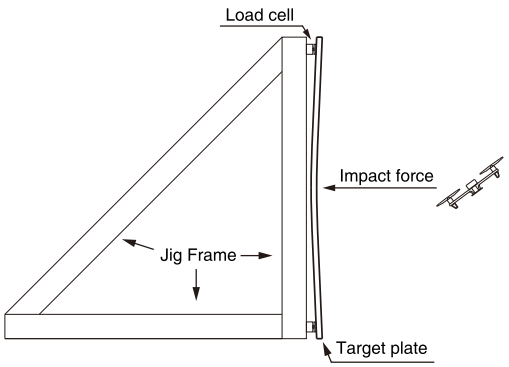

FIGURE 11. Schematic of the target deformation during collision.

the bending of the target and decreases with the recovery of the deformation of the target.

The force sensors used in the experiments were designed to measure only axial impact forces. Therefore, the bending moment induced by off-axis loading introduced errors in the measurement [36]. The measured tangential force was used to calibrate the normal force measured in the experiments due to the bending moment induced by the off-axis impact location. The force in the tangential directions (x and y) were taken into consideration using the coefficient α to quantitatively scale their effect on the total impact force. By comparing the normal and tangential forces measured in the numerical analysis with those measured during the experiment, it was determined that the about 10% of the total tangential force was measured by the piezoelectric force sensor due to the

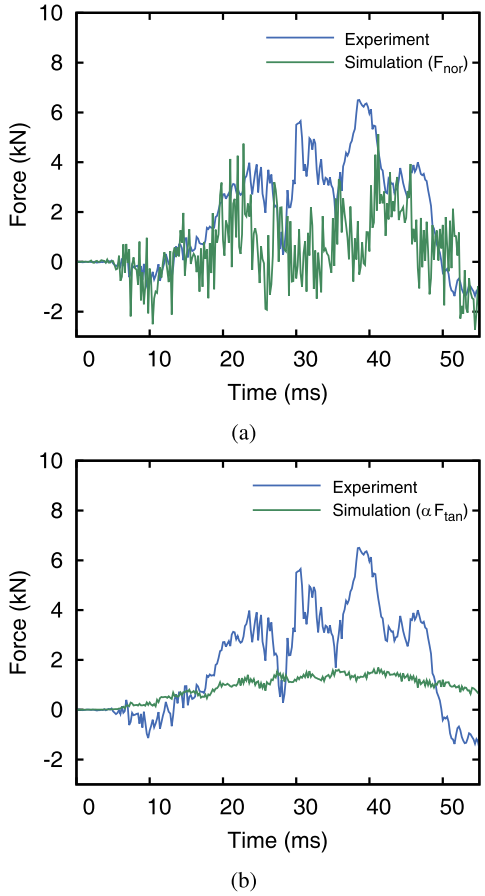

FIGURE 12. (a) Normal and (b) tangential forces in time.

bending moment. As a result, the total force applied to the force sensor was defined as $F_{tot} = F_{nor} + \alpha F_{tan}$ where F_{tot} is the total force, F_{nor} is the normal force, F_{tan} is the tangential force, and α is the tangential force coefficient with a value of 0.1.

When considering only the normal force, the third and fourth peak values in Fig. 13 were found to be underestimated compared to the test results, but the total impact force history indicates good agreement when considering the normal force together with the tangential force. Thus, the maximum impact forces from the numerical simulation and experiment are similar after considering the tangential forces. However, there still exist differences in the times at which the maximum forces occur due to the slightly different conditions in the field test and simulation. In the numerical analysis, the UAV has a perfectly symmetrical shape, and therefore flies without shaking. Consequently, the two front and two rear rotors collide with the glass panel at the same respective moments. However, in the experiment, it is not possible to perfectly synchronize the moments of collision. In fact, there is a short time difference between the collisions of each front rotor as well as each rear rotor. Overall, this discrepancy in impact moments does not significantly affect on the measured maximum impact forces.

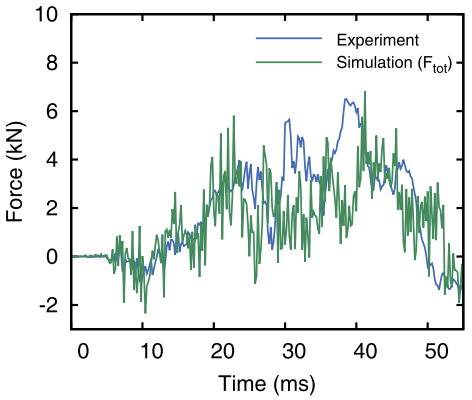

FIGURE 13. Total impact force time history considering normal and tangential forces.

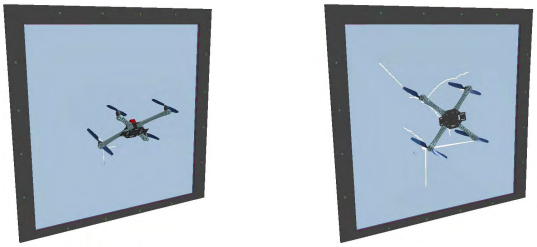

FIGURE 14. Crack initiation at the (a) front and (b) rear rotor impact for a 3 mm thick glass panel, impact velocity of 12.7 m/s, and impact angle of 36.7°.

2) UAV IMPACT SIMULATION WITH THINNER GLASS PANEL

A numerical simulation was also performed using 3 mm thick glass, an impact velocity of 12.7 m/s, and an impact angle of 36.7° to evaluate its consistency with an experiment of the same parameters in which the glass panel failed. As in the experimental observations, cracks were initiated in the glass panel due to the collision of the front rotor, and further fragmentation of the glass occurred at the collision position of the rear rotor, as can be seen in Fig. 14, confirming the accuracy of the numerical model.

V. SUMMARY AND CONCLUSIONS

In this study, we develop a new method for estimating UAV impact risk and evaluated it both experimentally and numerically. The blunt criterion is introduced and modified to estimate the probability of glass panel fracture by UAV collision. Using a series of impact tests, the failure modes and associated impact forces are evaluated, and a numerical model is developed and verified by comparison with the experimental results. We found that both the impact velocity and impact angle are major factors influencing the impact responses of glass. The results of the numerical analysis show that the time history of the impact force and the parameters that result in the destruction of the target are in good agreement with the experimental results. Thus the numerical model accurately predicts the responses of glass panels to UAV impact. It is expected that the results of the impact tests and modified blunt criterion presented in this paper will be useful in evaluating the collision risk presented by UAVs used in various fields, and further case studies of the numerical model will be performed to predict the risk of various impact cases that are difficult to evaluate in field tests. The current study was limited to the use of a single type of UAV, the DJI F450, weighing 903 g, due to time and budget constraints, but in order to advance the knowledge required for the comprehensive estimation of the damage due to UAV impact, further tests using different UAVs of various sizes and masses have been planned for future research. A sequential increase in the weight and size of UAVs will be beneficial by accumulating knowledge to form a basis for a comprehensive UAV impact study.

ACKNOWLEDGMENT

This research was supported by Ministry of Land, Infrastructure and Transport of Korean government under grant (18USTR-B127901-02) and was also supported by the National Research Foundation of Korea (NRF) grant funded by the Korea government (MSIT) (No.2018R1A2A1A05019453).

REFERENCES

[1] R. A. Clothier, J. L. Palmer, R. A. Walker, and N. L. Fulton, "Definition of an airworthiness certification framework for civil unmanned aircraft systems," *Saf. Sci.*, vol. 49, no. 6, pp. 871–885, 2011.
[2] R. Clarke, "The regulation of civilian drones' impacts on behavioural privacy," *Comput. Law Secur. Rev.*, vol. 30, no. 3, pp. 286–305, 2014.
[3] R. Clarke, "Appropriate regulatory responses to the drone epidemic," *Comput. Law Secur. Rev.*, vol. 32, no. 1, pp. 152–155, 2016.
[4] R. A. Clothier, B. P. Williams, and K. J. Hayhurst, "Modelling the risks remotely piloted aircraft pose to people on the ground," *Saf. Sci.*, vol. 101, pp. 33–47, Jan. 2018.
[5] R. Clothier, B. Williams, and A. Washington, "Development of a template safety case for unmanned aircraft operations over populous areas," in *Proc. SAE AeroTech Congr. Exhib. Soc. Automot. Eng.*, Sep. 2015, Paper 2015-01-2469.
[6] Y. Song, B. Horton, and J. Bayandor, "Investigation of UAS ingestion into high-bypass engines, part 1: Bird vs. drone," in *Proc. 58th AIAA/ASCE/AHS/ASC Struct. Struct. Dyn. Mater. Conf.*, 2017, p. 0186.
[7] K. Schroeder, Y. Song, B. Horton, and J. Bayandor, "Investigation of UAS ingestion into high-bypass engines, part 2: Parametric drone study," in *Proc. 58th AIAA/ASCE/AHS/ASC Struct. Struct. Dyn. Mater. Conf.*, 2017, p. 0187.
[8] D. Kaminski-Morrow. Cockpit windshields resilient to typical drone strikes: Analysis. Flightglobal. Accessed: Jul. 24, 2017. [Online]. Available: https://www.flightglobal.com/news/articles/cockpit-windshields-resilient-to-typical-drone-strik-439581/
[9] M. Huber. China conducts drone-aircraft collision tests. AINonline. Accessed: Dec. 14, 2017. [Online]. Available: https://www.ainonline.com/aviation-news/business-aviation/2017-12-14/china-conducts-drone-aircraft-collision-tests
[10] M. Johnson, J. Jung, J. Rios, J. Mercer, J. Homola, T. Prevot, D. Mulfinger, and P. Kopardekar, "Flight test evaluation of an unmanned aircraft system traffic management (UTM) concept for multiple beyond-visual-line-of-sight operations," in *Proc. 12th USA/Eur. Traffic Manage. Res. Develop. Seminar*, 2017.
[11] H. Pham, S. A. Smolka, S. D. Stoller, D. Phan, and J. Yang, "A survey on unmanned aerial vehicle collision avoidance systems," 2015, *arXiv:1508.07723*. [Online]. Available: https://arxiv.org/abs/1508.07723
[12] C. W. Tsang, K. C. S. Kwok, and P. A. Hitchcock, "Wind tunnel study of pedestrian level wind environment around tall buildings: Effects of building dimensions, separation and podium," *Building Environ.*, vol. 49, pp. 167–181, Mar. 2012.
[13] K. Dalamagkidis, K. P. Valavanis, and L. A. Piegl, "Evaluating the risk of unmanned aircraft ground impacts," in *Proc. 16th Medit. Conf. Control Automat.*, 2008, pp. 709–716.

[14] K. Dalamagkidis, K. P. Valavanis, and L. A. Piegl, "Current status and future perspectives for unmanned aircraft system operations in the US," *J. Intell. Robotic Syst.*, vol. 52, no. 2, pp. 313–329, 2008.
[15] A. La Cour-Harbo, "Mass threshold for 'harmless' drones," *Int. J. Micro Air Vehicles*, vol. 9, no. 2, pp. 77–92, 2017.
[16] A. La Cour-Harbo, "Quantifying risk of ground impact fatalities for small unmanned aircraft," *J. Intell. Robot. Syst.*, vol. 93, nos. 1–2, pp. 367–384, Feb. 2019.
[17] J. Cho and Y. Yoon, "How to assess the capacity of urban airspace: A topological approach using keep-in and Keep-out geofence," *Transp. Res. C, Emerg. Technol.*, vol. 92, pp. 137–149, Jul. 2018.
[18] J. D. Stevenson, S. O'Young, and L. Rolland, "Estimated levels of safety for small unmanned aerial vehicles and risk mitigation strategies," *J. Unmanned Vehicle Syst.*, vol. 3, no. 4, pp. 205–221, 2015.
[19] D. Floreano and R. J. Wood, "Science, technology and the future of small autonomous drones," *Nature*, vol. 521, no. 7553, pp. 460–466, 2015.
[20] A. Washington, R. A. Clothier, and J. Silva, "A review of unmanned aircraft system ground risk models," *Prog. Aerosp. Sci.*, vol. 95, pp. 24–44, Nov. 2017.
[21] C. H. Koh, K. Low, L. Li, Y. Zhao, C. Deng, S. K. Tan, Y. Chen, B. C. Yeap, and X. Li, "Weight threshold estimation of falling UAVs (Unmanned Aerial Vehicles) based on impact energy," *Transp. Res. C, Emerg. Technol.*, vol. 93, pp. 228–255, Aug. 2018.
[22] E. T. Campolettano, M. L. Bland, R. A. Gellner, D. W. Sproule, B. Rowson, A. M. Tyson, S. M. Duma, and S. Rowson, "Ranges of injury risk associated with impact from unmanned aircraft systems," *Ann. Biomed. Eng.*, vol. 45, no. 12, pp. 2733–2741, Dec. 2017.
[23] X. Zhang, H. Hao, and G. Ma, "Parametric study of laminated glass window response to blast loads," *Eng. Struct.*, vol. 56, pp. 1707–1717, Nov. 2013.
[24] *Standard practice for Determining Load Resistance of Glass In Buildings*, Standard Rev. E1300-09a, ASTM, West Conshohocken, PA, USA, 2009.
[25] *Minimum Antiterrorism Standards For Buildings*, Standard Rev. UFC 4-010-01, Department of Defense, Washington, DC, USA, 2018.
[26] L. M. Sturdivan, D. C. Viano, and H. R. Champion, "Analysis of injury criteria to assess chest and abdominal injury risks in blunt and ballistic impacts," *J. Trauma Injury, Infection Crit. Care*, vol. 56, no. 3, pp. 651–663, 2004.
[27] J. D. Riera, "On the stress analysis of structures subjected to aircraft impact forces," *Nucl. Eng. Des.*, vol. 8, no. 4, pp. 415–426, 1968.
[28] T. Sugano, H. Tsubota, Y. Kasai, N. Koshika, S. Orui, W. A. von Riesemann, D. C. Bickel, and M. B. Parks, "Full-scale aircraft impact test for evaluation of impact force," *Nucl. Eng. Des.*, vol. 140, no. 3, pp. 373–385, 1993.
[29] K.-J. Bathe, *Finite Element Procedures*. Berlin, Germany: Klaus-Jurgen Bathe, 2006.
[30] H. J. Mertz, P. Prasad, and G. Nusholtz, "Head injury risk assessment for forehead impacts," SAE Technical Paper, Tech. Rep. 960099, 1996.
[31] A. V. Shelley, "A model of human harm from a falling unmanned aircraft: Implications for UAS regulation," *Int. J. Aviation Aeronaut. Aerosp.*, vol. 3, no. 3, p. 1, 2016.
[32] J. O. Hallquist, *LS-DYNA Theory Manual*. Livermore, CA, USA: Livermore Softw. Technol. Corp., 2006.
[33] A. A. Griffith, "The phenomena of rupture and flow in solids," *Philos. Trans. Roy. Soc. A, Math. Phys. Eng. Sci.*, vol. 221, pp. 163–198, Jan. 1921.
[34] M. Overend, G. A. Parke, and D. Buhagiar, "Predicting failure in glass—A general crack growth model," *J. Struct. Eng.*, vol. 133, no. 8, pp. 1146–1155, 2007.
[35] M. Overend, S. De Gaetano, and M. Haldimann, "Diagnostic interpretation of glass failure," *Struct. Eng. Int.*, vol. 17, no. 2, pp. 151–158, 2007.
[36] O. Mack, "A new calibration method with static loads for piezoelectric force transducers," in *Proc. 18th IMEKO WORLD Congr. Metrol. Sustain. Develop.*, Rio de Janeiro, Brazil, 2006.

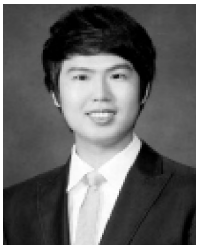

SANG EON LEE received the B.S. degree from the Department of Mechanical Engineering, Korea Advanced Institute of Science and Technology, Daejeon, South Korea, in 2014, where he is currently pursuing the Ph.D. degree in the Department of Civil and Environmental Engineering. His current research interests include the risk analysis of UAV, nonlinear waves, and nondestructive testing.

JAE-WOOK JUNG received the bachelor's degree from Hongik University, Seoul, South Korea, in 2012, and the master's degree from the Korea Advanced Institute of Science and Technology (KAIST), Daejeon, South Korea, in 2014, where he is currently pursuing the Ph.D. degree in civil and environmental engineering. His current research interest includes the impact risk assessment of the UAV.

YOUNGJUN CHOI received the B.S. degree in civil engineering from Hongik University, Seoul, South Korea, in 2016. He is currently pursuing the M.S. degree in civil and environmental engineering at the Korea Advanced Institute of Science and Technology (KAIST), Daejeon, South Korea. His current research interest includes the impact risk assessment of the UAV.

YOON-JIN YOON (M'17) received the B.S. degree in mathematics from Seoul National University, South Korea, the M.S. degree in computer science and management science and engineering from Stanford University, USA, and the Ph.D. degree in civil and environmental engineering from the University of California at Berkeley, USA, in 2010. She has been an Associate Professor with the Department of Civil and Environmental Engineering, Korea Advanced Institute of Science and Technology (KAIST), South Korea, since 2011. Before arriving at KAIST, she was a Graduate Student Researcher with the National Center of Excellence in Air Transportation Operations Research (NeXTOR), University of California at Berkeley, from 2005 to 2010. Previous research experience includes Research Assistant at the Artificial Intelligence Center, SRI International, Menlo Park, CA, USA, in 1999, and the Center of Reliability Computing, Stanford University, USA, from 2000 to 2002. Her main research area includes the traffic management of both manned and unmanned vehicles. Her recent research efforts include UAV traffic flow management and topological traffic network analysis using large scale driving data.

JUNG-WUK HONG received the bachelor's degree from Yonsei University, South Korea, in 1994, the master's degree from the Korea Advanced Institute of Science and Technology (KAIST), in 1996, and the Ph.D. degree in civil and environmental engineering from the Massachusetts Institute of Technology (MIT), in 2004. He was a Senior Research Engineer at the Weidlinger Associates, Inc., Mountain View, CA, USA, from 2006 to 2008, and a Manufacturing/Reliability Engineer with Cisco Systems, Inc., San Jose, CA, USA, in 2008. From 2008 to 2012, he was an Assistant Professor with Michigan State University. From 2012, he has been an Associate Professor at KAIST. His current research interests include particle-based methods, nonlinear wave propagation, and the failure analysis of structures under extreme events.